SHEAR STRENGTH OF ONE-WAY RIBBED SLABS WITH STEEL FIBER CONCRETE

LAJES NERVURADAS UNIDIRECIONAIS DE CONCRETO ARMADO COM FIBRAS DE AÇO AO CISALHAMENTO

LOSAS NERVADAS UNIDIRECCIONALES DE CONCRETO ARMADO CON FIBRAS DE ACERO AL CORTANTE

https://doi.org/10.56238/sevened2026.008-245

Felipe da Silva Leite[1], Leomir Rafael Brito Silva[2], Dênio Ramam Carvalho de Oliveira[3], Mateus Antônio Nogueira Oliveira[4], Marcio Rodrigo Nunes de Souza[5], Williander de Almeida Marques[6], Francisco Xavier Gomes Pantoja Junior[7], Edson Igreja Bentes[8]

ABSTRACT

The ribbed slabs are used both in small and large constructions, and its use is growing due to the advantages that this constructive system provides. However, considering the demeanor of these slabs without transverse reinforcements (stirrups), few studies were made in Brazil. This study brings an experimental analysis of 8 unidirectional ribbed slabs of reinforced concrete subjected to loads perpendicularly distributed to the ribs. 4 (four) reference slabs and 4 (four) reinforced slabs with steel fibers with a length of 1,700 mm and width ranging from 650 to 950 mm were tested, all with table thickness of 40 mm and ribs with cross section of (100 x 100) mm². The compressive strength of concrete was approximately of 30 MPa. The results were compared to those estimated by the design codes ACI 318 [1], EHE 08 [2], NBR 6118 [3] and MC10 [4]. It was verified that the increase in shear and bending strength of the reinforced slabs with fibers was substantial, what makes those slabs technically feasible.

Keywords: Ribbed Slab. One-Way Slab. Shear. Steel Fiber.

RESUMO

Lajes nervuradas são empregadas tanto em pequenas quanto em grandes obras e sua utilização cresce face as vantagens que este sistema construtivo proporciona. Entretanto, poucos estudos foram realizados no Brasil considerando o comportamento destas lajes sem

[1] Master's degree in Structures and Civil Construction. Universidade Federal do Pará. E-mail: felipe.leite@ifap.edu.br
[2] Civil Engineer. Universidade Federal do Pará. E-mail: sgt.rafa@gmail.com
[3] Dr. in Structures. Universidade Federal do Pará. E-mail: denio@ufpa.br
[4] Dr. in Civil Engineering. Universidade Federal de Minas Gerais. E-mail: mateusantonio@ufmg.br
[5] Dr. in Structures and Civil Construction. Instituto Federal do Amapá. E-mail: marcio.souza@ifap.edu.br
[6] Civil Engineer. Universidade Federal do Amapá. E-mail: williandermarques@gmail.com
[7] Civil Engineer. Universidade Federal do Amapá. E-mail: francisco.pantoja@ifap.edu.br
[8] Civil Engineer and Occupational Safety Engineer. Universidade Federal do Amapá. E-mail: edson.bentes@ifap.edu.br

armaduras transversais (estribos), nas nervuras. Este trabalho apresenta uma análise experimental de 8 lajes nervuradas unidirecionais de concreto armado sujeitas a carregamentos distribuídos perpendicularmente às nervuras. Foram ensaiadas 4 (quatro) lajes de referência e 4 (quatro) lajes reforçadas com fibras de aço com comprimento de 1.700 mm e largura variando de 650 a 950 mm, todas com espessura de capa de 40 mm e nervuras com seção transversal de (100 x 100) mm². A resistência do concreto à compressão foi de aproximadamente 30 MPa. Os resultados foram comparados aos estimados pelas normas ACI 318 [1], EHE 08 [2], NBR 6118 [3] e MC10 [4]. Verificou-se aumento de resistência considerável ao cisalhamento e a flexão para as lajes reforçadas com fibra, tornando-as tecnicamente viáveis.

Palavras-chave: Laje Nervurada. Laje Unidirecional. Cisalhamento. Fibra de Aço.

RESUMEN

Las losas nervadas se emplean tanto en obras pequeñas como en grandes, y su uso crece debido a las ventajas que este sistema constructivo proporciona. Sin embargo, pocos estudios se han realizado en Brasil considerando el comportamiento de estas losas sin armaduras transversales (estribos) en las nervaduras. Este trabajo presenta un análisis experimental de 8 losas nervadas unidireccionales de concreto armado sometidas a cargas distribuidas perpendicularmente a las nervaduras. Se ensayaron 4 (cuatro) losas de referencia y 4 (cuatro) losas reforzadas con fibras de acero, con longitud de 1.700 mm y ancho variando entre 650 y 950 mm, todas con un espesor de capa de 40 mm y nervaduras con sección transversal de (100 × 100) mm². La resistencia a compresión del concreto fue de aproximadamente 30 MPa. Los resultados se compararon con los estimados por las normas ACI 318 [1], EHE 08 [2], NBR 6118 [3] y MC10 [4]. Se verificó un aumento considerable de la resistencia al corte y a la flexión en las losas reforzadas con fibra, haciéndolas técnicamente viables.

Palabras clave: Losa Nervada. Losa Unidireccional. Corte. Fibra de Acero.

1 INTRODUCTION

Currently, due to the demands of projects, the construction industry demands a growing need for larger spans and fewer beams. In this scenario, the use of ribbed slabs stands out, which, in turn, are lighter structures due to the use of expanded polystyrene (EPS), or even removable formwork in regions below the neutral line, where, in the case of solid slabs, this region would be filled with concrete, making the latter less economical, having to use part of its resistant capacity to combat self-weight and even increase the number of beams in order to reduce the arrows. According to Bochi Júnior (1995) [5], the use of ribbed slabs, due to the minimization of costs and deadlines, met the growing need for rationalization in civil construction.

Unidirectional ribbed slabs can be built in a precast way, totally or only ribbed, and this brings benefits, such as the reduction of material for the execution of form and shoring, reduction of labor for execution, shorter time for execution compared to conventional ones, lower concrete consumption due to the area filled by inert materials and reduction in the amount of debris on site, caused by wood discards. Despite the advantages mentioned, the elimination of beams, due to the gain in span increase provided by ribbed slabs, causes some disadvantages, such as the decrease in the overall stability of the structure, due to horizontal actions.

The importance of this study is to analyze the results of stresses, strains and displacements, intending to expand the knowledge about the shear resistant behavior of ribs and layers, considering the variation of the distance between rib axes () l_0and the use of steel fiber reinforced concrete (CRFA), seeking to qualify and quantify the contribution of the system to the gain in shear strength. It seeks to evaluate the benefits of the use of steel fiber reinforced concrete (CRFA) in reinforced concrete ribbed slabs from experimental studies where the distance between the rib axes was the main variable, pointing out the influence of this variation on their behaviors and the advantages caused by the addition of steel fiber to concrete, as well as to evaluate the level of precision of the normative codes in relation to the shear strength of structures. It is noteworthy that Barros et al. (2003) [6] and Gava (2004) [7], have already verified the contribution of fibers as reinforcement and Claudio et al. (2014) [8] presents the technological advances in the development of fibers for concrete reinforcement.

2 LITERATURE REVIEW

2.1 STRUCTURAL BEHAVIOR

The improvement of the quality of design procedures related to shear is a concern of structural engineering. Shear failures in reinforced concrete structures usually occur in a fragile way, with little or no prior warning, in addition, they tend to be less predictable than flexural failures, due to the considerably more complex failure mechanisms. Unidirectional ribbed slabs characteristically present T-beam configurations with joined tables, requiring an understanding of the shear stresses and shear forces that will arise from external stresses. According to Rüsch (1960) [9], shear cracks can originate from flexural cracks. In these cases, these flexural cracks, as soon as they appear, trigger a considerable redistribution of internal stresses with consequences that are difficult to calculate and that influence the inclination of the shear cracks.

2.2 RESISTANT MECHANISMS

According to Rombach and Latte (2008) [10], the determination of the shear resistant capacity in reinforced concrete structures without transverse reinforcement is a classic structural problem studied for more than 100 years, and this difficulty consists in the quantification of the strength that compressed concrete can offer in the face of stresses. Despite this work, most of the research focuses on simply supported beams or on slabs covering strips with loads applied over the total width b less than $4 \cdot d$, with the useful height of the slab. Experimental studies show that the shear resistant capacity of a reinforced concrete beam can be divided into two parts: one resisted by the transverse reinforcement and the other by the concrete and its auxiliary mechanisms, which will be addressed in this item. That is, a beam, even without stirrups, has the ability to resist a certain shear force. Macgregor (1997) [11] shows the contribution of the various components of the shear strength mechanisms of unreinforced beams, except for the component relating to the arc effect, as shown in Figure 1. When the beam is stressed, the shear is transferred through the ABC line by the concrete strength mechanisms: uncracked concrete ($(V_{cy}$), aggregate meshing (V_a) and longitudinal reinforcement pegging (V_d). Immediately after the bending cracks are inclined, between 40% and 60% of the total shear strength is resisted by the joint work of V_d and V_{cy}. Considering the DEF part of the fissured structure and assuming the moments with respect to point E, we have that V_d and $V_a$cause momentum with respect to point E, which must be balanced by the compressive force C'1. The equilibrium of the horizontal resultant in the ABDE section shows that T1 = C1 + C'1, and finally, T1 = C1 + C'1 should balance the external momentum of this section. As the diagonal crack progresses,

the plot decreases, V_a increasing the fraction resisted by V_{cy} and V_d . The dowel, $V_d$leads to the separation of the concrete along the reinforcement. When the crack occurs, it falls, approaching zero. When V_a and V_d disappear, then V_{cy} and C1 causes the result of all the shear and compression to be transmitted to the AB depth above the crack. At this point in the life of the structure, the AB section being too shallow, will not withstand the compressive forces required for balance. As a result this section crushes upwards, bringing no resistance to the stress. Collins et. al (2008) [12] present a review analysis of 60 years of research on the behavior of short reinforced concrete beams without stirrups, where it was concluded that the largest portion of shear strength is not found in the characteristic strength of concrete, but is affected by the dimensions of the structural element, the meshing of the aggregates and the pin effect of the longitudinal reinforcement. According to ACI-ASCE (1973) [13], for reinforced concrete structures subjected to shear stresses, the portion of strength due to concrete is the sum of several mechanisms capable of transmitting forces between sections, such as:

Aggregate interlock: this mechanism occurs between the two surfaces caused by a crack. The contribution of aggregate meshing to shear strength depends on crack opening and surface roughness;

Arching action: this mechanism occurs more expressively in beams with reduced spans due to the accommodation of compressive stresses in the arc and the intensity of these stresses depends mainly on the inclination of the arc, being directly linked to the a/d ratio, that is, the lower the value of the shear span a (short beams), the greater the arc effect;

Cantilever action: this mechanism occurs in uncracked sections of the beam (between two consecutive cracks) or in non-cracked parts of cracked elements (compression zone of a cracked section);

Dowel action-effect: Longitudinal reinforcement resists a portion of the displacement caused by shear force due to the pin effect on the bar. The pin force on the longitudinal reinforcement bar depends on the stiffness of the bar at the intersection with the crack.

2.3 PROPERTIES OF CRFA IN THE HARDENED STATE

Ductility, toughness and post-crack residual strength are some of the advantages of CRFA, compared to simple concrete. The distinct behavior between these materials can be attributed to the fiber-concrete interaction that develops at the time of crack formation. At this time, there is a transfer of forces between the concrete and the fibers. To explain this mechanism of stress transfer, Garcez (2005) [14] shows in Figure 2 that, after the occurrence of a crack (phase 5), the transfer of forces occurs by friction, and this frictional stress is

distributed at the fiber-concrete interface. For stress levels higher than the formation of a crack, the displacement of the fibers occurs (phase 4) and the process of tearing the fibers from the concrete mass begins (phase 2). At this moment, the effort for the fiber to be pulled out is high, which justifies the tenacity of CRFA. When the stress intensifies, the crack opening increases and the fibers begin to act as stress transfer bridges (phase 3) until their total pullout or rupture (phase 1 and 2, respectively).

2.4 FIBER-REINFORCED BEAMS AND SLABS

According to Hazrina et al (2017) [15], concrete reinforced with steel fibers with fiber consumption (C_f) of 1%, can fully replace conventional reinforcements, both bending and shear, with a load capacity practically equal to slabs with reinforcement. For Arslan (2014) [16], in concrete beams reinforced with steel fibers, the control of cracking resulting from normal stress is more effective compared to simple concrete, as the fibers provide greater rigidity after the onset of cracking. According to Macgregor and Whigt (2012) [17], steel fibers tend to increase the shear capacity by ensuring a tensile strength of the concrete along the inclined crack, resulting in an increase in the aggregate mesh component, similar to that observed in beams with transverse reinforcement. According to KWAK et al (2002) [18], the use of steel fiber-reinforced concrete in beams increases the shear strength, and the rupture, which is usually brittle, can be suppressed in favor of a ductile rupture. As previously mentioned, steel fibers help to form tension bridges that perform a greater distribution of forces, helping as a mechanism that slows down the propagation of cracks in concrete, providing greater bearing capacity (Dinh et al., 2010) [19].

To formulate the equilibrium condition for a steel fiber-reinforced, unstirruped, reinforced concrete beam, Lim and Oh (1999) [20] showed what is required to identify all the external and internal actions that may be present on the face of the inclined crack. The shear forces are transmitted through the following plots: effect of the uncracked concrete of the compressed region (V_c), effect of the meshing between the aggregates along the diagonal crack (V_a), pin effect of the longitudinal reinforcement that crosses this crack (V_d) and vertical components of the pullout force of the fibers along the inclined crack (V_f).

3 NORMATIVE RECOMMENDATIONS

3.1 NBR 6118 (2023)

According to the Brazilian standard, unidirectional ribbed slabs must be calculated according to the direction of the ribs, disregarding the transverse stiffness and torsional stiffness, this standard does not bring prescriptions for the calculation of slabs manufactured

with CRFA. NBR 6118 [3] prescribes that for ribbed slabs with spacing (l_0) between rib axes less than or equal to 650 mm, the verification of the bending of the table may be waived, and for the verification of the shear of the rib region, the consideration of the slab criteria (Equation 1) is allowed, in relation to the term (σ_{CP}), this was equated to zero since the tested slabs were not subjected to preloads or compressive stresses perpendicular to the cross-section. For slabs with rib axis spacing between 650 mm and 110 mm, the bending of the table is required, and the ribs must be checked for shear as beams, checking the tensile diagonal, (Equation 2). For the two equations, the weighting coefficient of concrete (γ_c) was not usedγ_c, and the values of concrete, tensile and compressive strength were those found in the characterization tests, (f_c) and (f_c) presented in Table 1, aiming at the comparison between the equations and the experimental results.

$$V_{Rd} = [\tau_{Rd} \cdot k \cdot (1{,}2 + 40 \cdot \rho_l) + 0{,}15 \cdot \sigma_{CP}] \cdot b_w \cdot d \quad \text{Equation 1}$$

$$V_{Rd} = V_{c0} = 0{,}6 \cdot f_{ctd} \cdot b_w \cdot d \quad \text{Equation 2}$$

$$\rho_l = \frac{A_{sl}}{b_w \cdot d} \leq 0{,}02 \quad \text{Equation 3}$$

$$k = (1{,}6 - d) \geq 1 \quad \text{Equation 4}$$

$$f_{ctk,inf} = 0{,}7 \cdot f_{ct,m} \quad \text{Equation 5}$$

$$f_{ct,m} = 0{,}3 \cdot {f_{ck}}^{2/3} \quad \text{Equation 6}$$

$$f_{ct,d} = \frac{f_{ctk,inf}}{\gamma_c} \quad \text{Equation 7}$$

$$\tau_{Rd} = 0{,}25 \cdot f_{ct,d} \quad \text{Equation 8}$$

Where as:

f_c: Compressive strength of concrete;

f_t: Tensile strength of concrete;

f_{ck}: Characteristic compressive strength of concrete;

V_{Rd}:: Calculation resistant shear force;

V_{c0}: Reference value for the portion of shear force resisted by the concrete;

ρ_l: Geometric longitudinal reinforcement rate of tensile;

τ_{Rd}:Shear stress resistant calculation;

f_{ctd}: Tensile strength of concrete;

σ_{CP}: : initial stress in the concrete at the level of the barycenter of the prestressing reinforcement, due to the simultaneous prestressing of n cables;

γ_c: Weighting coefficient of the strength of concrete;

$f_{ctk,inf}$ Characteristic tensile strength of concrete with the lower value;

$f_{ct,m}$: Average tensile strength of concrete ($f_{ct,m} = f_t$);

A_{sl}: Area of longitudinal tensile reinforcement;

k: Coefficient related to longitudinal tensile reinforcement;

b_w: Minimum width of the section along the usable height d.

3.2 ACI 318 (2014)

According to ACI 318 [1], the shear strength of unidirectional ribbed slabs of unshear reinforced reinforced concrete is based on the average shear stress of the effective cross-sectional surface $b_w \cdot d$ and the pin effect. For the calculation of beams without shear reinforcement, we have that V_u=V_c caccording to Equation 8 and the shear strength can be expressed by Equation 9.

$$V_u = V_c \qquad \text{Equation 8}$$

$$V_c = 0{,}16 \cdot \lambda \cdot \left(\sqrt{f'_c} + 17 \cdot \rho_w\right) \cdot b_w \cdot d \qquad \text{Equation 9}$$

Where as:

V_c : Resistance to the shear force absorbed by the concrete in N.mm;

V_u: Shear effort requested last in N.mm;

f'_c: Compressive strength of concrete in Mpa;

ρ_w: Longitudinal reinforcement ratio $(\rho_w = \rho_l)$;

λ: Stress modification factor in concrete (normal mass concrete λ=1))

3.3 EHE 08 (2010)

According to the Spanish standard EHE 08 [2], the shear strength of unreinforced concrete parts to shear (V_{u2}) is expressed by equation 10, where (V_{cu}) is estimated by equation 11 and the quantities (f_{cv}) and $(\mathcal{E})$ are estimated by equations 12 and 13, respectively. (V_{fu}) is the portion of strength absorbed by the steel fibers, calculated according to equation 9, the parameter (f_{R3}) is obtained with equation 29, in relation to equations 14, 15 and 16 the weighting coefficient () was not used (γ_c) in the calculation of $(f_{R3,d})$ and in (f_{cv}) experimental values presented in table 3 were used, in order to compare the results of the equations to the results obtained in the experimental tests. f_cv

$$V_{u2} = V_{cu} + V_{fu} \qquad \text{Equation 10}$$

$$V_{cu} = \frac{0{,}18}{\gamma_c} \cdot \varepsilon \cdot \left((100 \cdot \rho_l \cdot f_{cv})^{1/3} + 0{,}15 \cdot \sigma_{CP}\right) \cdot b_w \cdot d \geq 0{,}75 \cdot \varepsilon^{\frac{2}{3}} \cdot f_{cv}{}^{\frac{1}{2}} \cdot b_w \quad \text{Equation 11}$$

$$f_{cv} = \min(f_{ck}; 60) \quad \text{Equation 12}$$

$$\varepsilon = (1 + \sqrt{\frac{200}{d}}) \leq 2 \quad \text{Equation 13}$$

$$V_{fu} = 0{,}7 \cdot \varepsilon \cdot \tau_{fd} \cdot b_w \cdot d \quad \text{Equation 14}$$

$$\tau_{f,d} = 0{,}5 \cdot f_{ctR,d} \quad \text{Equation 15}$$

$$f_{ctR,d} = 0{,}33 \cdot f_{R3,d} \quad \text{Equation 16}$$

Where as:

V_{cu}: Contributionof concrete shear strength;

V_{fu}:Contribution of strength of steel fibers;

f_{cv}: Calculation resistance to shear stress $(f_{cv} = f_c)$;

$\mathcal{E}$: Relative deformation along the height of the section (scale factor);

τ_{fd}: Calculation value of the increase in shear strength due to the reinforcement of steel fibers;

$f_{ctR,d}$: Calculationof the residual tensile strength of CRFA;

$f_{R3,d}$: Calculation value of the residual tensile strength of the CRFA at the flexion corresponding to the crack opening of 2.5 mm.

3.4 CEB-FIP MODEL CODE (2010)

The CEB-FIP Model Code (MC10) is a document produced in collaboration with 41 countries, with the main objective of serving as a basis for future codes and presenting new developments regarding concrete materials and structures, in order to achieve optimal behavior, based on performance requirements.

3.4.1 Shear Strength (V_R)

The shear strength $(V_{Rd,f})$ of concrete parts not reinforced to shear and reinforced with steel fibers is established as a function $(V_{Rd,f})$ as shown in equation 17, where (f_{Ftuk}) defined by equation 18, (f_{Fts}) according to equation 19 and (f_{ctk}) according to equation 20. The estimated strength of non-fiber-reinforced concrete was estimated by equation 21 and the

parameters (k_V) and (k_{dg}) were estimated by equations 22 and 23, respectively. For all equations, the test values referring to the resistant characteristics of the concrete and the weighting coefficient γ_c were discarded in order to compare these equations with the experimental results presented in Table 4.

$$V_{Rd,f} = \left\{\frac{0{,}18}{\gamma_c} \cdot k \cdot \left[100 \cdot \rho \cdot \left(1 + 7{,}5 \cdot \frac{f_{Ftuk}}{f_{ctk}}\right) \cdot f_{ck}\right]^{1/3} + 0{,}15 \cdot \sigma_{CP}\right\} \cdot b_w \cdot d \geq 0{,}035 \cdot k^{1{,}5} \cdot {f_{CK}}^{0{,}5} \cdot b_w \cdot d \quad \text{Equation 17}$$

$$f_{Ftuk} = f_{Fts} - \frac{1{,}5}{2{,}5} \cdot (f_{Fts} - 0{,}5 \cdot f_{R3} + 0{,}2 \cdot f_{R1}) \geq 0 \quad \text{Equation 18}$$

$$f_{Fts} = 0{,}45 \cdot f_{R1} \quad \text{Equation 19}$$

$$f_{ctk} = 2 \cdot \ln\left(1 + \frac{f_{CK}}{10}\right) \quad \text{Equation 20}$$

$$V_R = K_V \cdot \frac{\sqrt{f_{ck}}}{\gamma_c} \cdot z \cdot b_w \quad \text{Equation 21}$$

$$k_V = \frac{0{,}4}{1 + 1500 \cdot \varepsilon_x} \cdot \frac{1300}{1000 + k_{dg} \cdot z} \quad \text{Equation 22}$$

$$k_{dg} = \frac{32}{16 + d_g} \geq 0{,}75 \quad \text{Equation 23}$$

Where as:

$V_{Rd,f}$: Shear strength of fiber-reinforced concrete;

f_{Ftuk}: Characteristic value of ultimate residual tensile strength for CRFA;

f_{ctk}: Characteristic value of tensile strength for fiberless concrete;

f_{Fts}: Residual resistance in the service limit state;

f_{R1}: Calculation value of the residual tensile strength of the CRFA at the flexion corresponding to the crack opening of 0.5 mm;

ε_x: Deformation in the center of the vein;

Z: Lever arm between the traction armature and the compression block;

d_g: Maximum aggregate diameter.

3.4.2 Flexural Strength

To determine the value of (M_R), the inflection model of (MC10) [4] was used. In this model, the contribution of steel fibers is given by (f_{Ftu}), which is calculated by equation 13. As shown in Figure 3, the quantities (F) and (y) are, respectively, the resulting forces and

their respective lever arms and, define the compression block, establish the values for the parameters $\lambda = 0{,}8$ and $\eta = 1$ for $f_c \leq 58\ MPa$.

Regarding the distribution of the strains, it is assumed that (ε_{cu}) is equal to 3.5‰ε_cu, but it is observed that ($\varepsilon t_{,bot}$) should not be greater than (ε_{fu}), estimated by equation 24. Admitting (S_{rm}) according to equation 27 leads to satisfactory answers. In this context, Table 5 presents a summary of the interactive process, as a function of the neutral line, after establishing the compatibility of the deformations and the equilibrium of the resulting forces ($\Sigma F \approx 0$).

$$\varepsilon_{fu} = \frac{w_u}{l_{cs}} \quad \text{Equation 24}$$

$$w_u = 2{,}5\ mm \quad \text{Equation 25}$$

$$l_{cs} = \min(y; S_{rm}) \quad \text{Equation 26}$$

$$S_{rm} = \frac{d}{2} \quad \text{Equation 27}$$

Where as:

Where as:

M_R: Moment resistant;

a: Shear span value;

ε_{fu}: Strain of non-metalic reinforcement at maximum force in tension;

l_{cs} Refers to the characteristic structural length;

w_u: Represents the maximum permissible crack opening;

S_{rm}: Value of the average distance between cracks;

y Represents the distance from the neutral line to the most tensile fiber of the section;

ε_{cu}: Maximum deformation in compressed concrete;

$\varepsilon t_{,bot}$: : Deformation in the most tensile fiber of the section.

4 EXPERIMENTAL PROGRAM

4.1 CHARACTERISTICS OF SLABS

Tests were carried out on 8 panels of unidirectional ribbed slabs of reinforced concrete until failure, without the presence of anti-shear reinforcement in the ribs. The slabs were divided into 2 groups of 4 slabs each, in which group C30 (Reinforced Concrete Slab) was composed of four panels of 1,700 mm in length, with variations in the distance between the rib axes (l_0) l_0of 550 mm, 650 mm, 750 mm and 850 mm and the CRFA group (Fiber-Steel Reinforced Concrete Slab), composed of four slabs with the same variation as the previous group, but containing steel fiber in the concrete, as shown in Table 1. All slabs had a

thickness of 40 mm for the layer and ribs with a cross-section of (100 x 100) mm², leaving them with a total height of 140 mm (Figures 4 and 5).

The concrete cover adopted for all reinforcements was 20 mm. All panels have the same arrangements for the reinforcements, consisting of 2Ø12.5 mm in the ribs, at a useful height of 113.8 mm, resulting in a 2.06% reinforcement rate and with ratio $a/d = 3{,}08$, and with bars of 5 mm diameter to combat the bending of the tables. Shear reinforcement was not used in the ribs in order to quantify the contribution of the spacing between the ribs and steel fibers to the shear strength. To avoid localized crushing of the concrete due to the concentration of stresses in the regions of support and application of the load, it was decided to reinforce these locations using stirrups 2Ø6.3 mm in diameter and 100 mm apart from each other in the region of the supports and points of application of the load, figures 4 and 5 show the arrangements of the reinforcements. Figure 6 shows the steel fiber used in the reinforcement of the CRFA slabs, which was the Crimped type (Harvest W-LCS/50/75W) with a length (l_f) l_fof 38 mm and equivalent diameter (d_f) of 1.28 mm, characteristics determined according to NBR 15530 [21], and tensile strength limit of 800 MPa.

With regard to the compressive strength of the concrete (f_c), MPa was adopted and the concreting of the slabs was carried out with concrete made in situ, together with the addition of steel fiber, requiring an approximate volume of 1 m³ to mold the slabs and the specimens. Figure 7 shows the stages of making the ribbed slabs.

4.2 INSTRUMENTATION

The instrumentation aimed to record the behavior of the slabs for later comparison, in order to identify the influence of the steel fibers on the shear performance and define the failure modes. For this purpose, the displacements and deformations in the reinforcements and concrete were monitored, in addition to the mapping of the cracks.

4.2.1 Displacements

The vertical displacements (deflects) were measured using 2 DIGIMESS dial indicators, with a maximum reading stroke of 50 mm and a precision of 0.01 mm, positioned in the middle of the span, spaced from one rib to the other and in contact with the upper surface of the slabs. In the lower part of the slab, near the center, an LVDT (Linear Variable Differential Transformer) of the DCTH3000A type, manufactured by the company RDP Electrosense, with a linear displacement of ±75 mm, positioned with the help of a magnetic support fixed to the reaction beam of the test frame, was used. Figure 8 shows the positioning of the indicator clocks.

4.2.2 Concrete surface

To measure the deformations in the concrete, 8 electric resistance extensometers (EER) were used, manufactured by the company EXCEL SENSORES, model PA-06-201BA-120L, one for each slab, fixed to the upper surface of the concrete, just above one of the ribs, in the middle of the span of these, and later connected to the data acquisition equipment (ALMEMO model). Such positioning is justified by the fact that it is the region of maximum bending moment, that is, the region of maximum compressive stress of the concrete. The positioning of the extensometers on the concrete surface is shown in Figure 8.

4.2.3 Bending Armor

The instrumentation of the flexural reinforcement was carried out by means of 8 electric resistance extensometers (EER), manufactured by the company EXCEL SENSORES, model PA-06-125AA-120L, which were fixed to one of the flexural reinforcement bars and in the middle of the span of a rib of each slab, as shown in Figure 8. Again, this position is justified by the fact that it is the region of maximum bending moment where the flow of the tensile reinforcements occurs.

4.3 TEST SYSTEM

The test system was mounted on a reaction slab and aimed at the response of the structure to the distributed loading, applied transversely to the ribs. Thus, the slabs were supported on rollers on metal beams, supporting the load applied perpendicular to the ribs (horizontal direction), on the upper face of the panel, through a bi-supported metal profile used for load distribution. The application of the loading took place through a manually operated hydraulic cylinder with a capacity of 1000 kN, connected to a hydraulic pump, and the recording of the loading intensity was carried out with the aid of a load cell with a capacity of 1000 kN and an accuracy of 1 kN connected to a digital display. The loads were established by 5 kN load steps.

The strain readings were obtained using a modular data acquisition system ALMEMO ®5690-2 m, from Ahlborn, compatible with the AMRWinControl software, which read the strain gauges positioned on the steel and concrete. Load increment intervals of 5 kN were used for each data collection, as well as for the proper reading of extensometers, indicator clocks and crack marking, in order to achieve a satisfactory number of readings aiming at the execution of the graphs that will represent the behavior of the slabs. Figure 9 shows details of the test system.

5 RESULTS

5.1 MATERIALS

The mechanical properties of the concrete were determined from compressive strength (f_c),ctensile strength (f_t) by diametrical compression and modulus of elasticity (E_c) tests, according to the standards NBR 5739 [22], NBR 7222 [23] and NBR 8522 [24], respectively. The results presented in Table 2 are the average for 3 cylindrical specimens tested for each slab at their respective ages.

The characteristics of tensile steel were obtained through standardized tests and a normal distribution curve. Three 600 mm long specimens were extracted for the tensile tests, all from the same batch, with 12.5 mm diameter (CA-50), in order to determine the mechanical properties of the steel, such as yield stress (f_{ys}) equal to 570 MPa, rupture stress (f_u) equal to 687 MPa, yield strain (ε_{ys}) equal to 2.33 and modulus of elasticity (E_S) of 244.6 GPa.

Regarding steel fibers, the proposal by Moraes Neto et al. (2013) [25] to estimate the values of residual stresses (f_{Ri}=1, 3 and 4), used in the estimates of the load capacity of the slabs and this relates the fiber consumption (C_f) with the product between the fiber length (l_f) and the diameter (d_f) as follows:

$$f_{R1} = 7{,}5 \cdot (C_f \cdot \frac{l_f}{d_f})^{0{,}8} \qquad \text{Equation 28}$$

$$f_{R3} = 6{,}0 \cdot (C_f \cdot \frac{l_f}{d_f})^{0{,}7} \qquad \text{Equation 29}$$

5.2 DISPLACEMENTS

The indicator clocks were distributed in the middle of the rib span and the cover, in order to compare the behavior of the slabs due to the variation in the spacing between the ribs. Figure 10 shows the graph of the vertical displacements observed in the slabs. There was a greater displacement, until failure, in the CRFA-reinforced slabs compared to the C30 class slabs, on average 37% of increase, and this increase in ductility is explained by the crack control caused by the interaction of the fiber with the concrete. The displacement graphs also show an increase in stiffness provided by the increase in the modulus of elasticity of CRFA concrete.

5.3 CONCRETE DEFORMATIONS

It was decided to measure only the deformations in the rib region and the L1 and L6 slabs were the ones that presented the highest deformations, 1.1‰ ($\varepsilon c_{,máx}$), indicating that there was no concrete crushing in any of the slabs, as shown in Table 3.

5.4 BENDING REINFORCEMENT DEFORMATIONS

The highest deformations were recorded for the slabs with higher failure loads, all reinforced with CRFA (L6, L7 and L8), probably due to the increase in ductility of the concrete, generating greater displacements. The L8 slab showed a maximum deformation of 2.69‰ ($\varepsilon_{s,máx}$) in the flexural reinforcement, reaching the yield (2.33‰), being the only one to flow. Figure 11 shows the maximum deformations in the bending reinforcements for all slabs.

5.5 CRACKING PATTERN

The cracking pattern was similar for all slabs, where the beginning occurred with cracking in the center of the layers towards the ribs. In the ribs, inclined shear cracks occurred in the region of the supports, which configured the imminence of shear failure, and the rupture surface extended to the layer, leading to the collapse of the slab.

On the upper surface of the slab there was a longitudinal cracking pattern at the meeting between the layer and the rib, and in some slabs this crack reached the cross-section of the rib. This cracking on the upper surface is predicted by the standards for ribbed slabs with a wheelbase ((l_0) above 650 mm, however, below this normative value there is no recommendation for analysis, and the layers of the L1 and L5 slabs presented this cracking parallel to the ribs excessively. The cracking patterns of the ribs of the slabs are shown in Figure 12. These veins showed a higher degree of cracking than the layers and were where the ruptures occurred.

5.6 ULTIMATE LOADS AND BURST MODES

The tested ribbed slabs reached failure with loads (P_u) of 116 kN, 95 kN, 91 kN, 107 kN, 118 kN, 140 kN, 178 kN and 186 kN for slabs L1 to L8 respectively, as shown in Figure 13. Based on previous studies carried out with ribbed slabs, the relevant influence of the screed stiffness on the shear strength of ribbed slabs was perceived, as already evidenced by Souza et al. (2014) [26].

There was a proportionality between the use of CRFA, with the distance between the ribs (l_0) and the increase in the ultimate breaking load, demonstrating that there was a

considerable gain in strength even without transverse reinforcement. All slabs failed by shear without showing yield of the rib flexural reinforcement, with the exception of L8. The value of the ultimate bending load (P_{FLEX}) was 176 kN, estimated by the CEB-FIP standard (MC10) [4], according to the interactive process presented in table 5, only the L7 and L8 slabs presented rupture loads (P_u) uwith values close to (P_{FLEX}), for the other slabs the values of the rupture loads (P_u) , were lower than (P_{FLEX}), ratifying the observed failure mode. Table 3 presents the observed rupture modes and the relationship between P_{FLEX}/P_u.

5.7 COMPARISON BETWEEN EXPERIMENTAL AND ESTIMATED RESULTS

Table 4 presents the last experimental loads and estimated by the standards ACI 318 [1], EHE 08 [2], NBR 6118 [3] and MC10 [4] for shear strength (V_U), all standards, were used to estimate the strength of slabs made with concrete of class C30 and presented conservative results with regard to shear, on average, the results of NBR 6118 [3] were 40% lower than the experimental results and the results estimated by ACI 318 [1] were more conservative with results on average, 56% lower, compared to the experimental results. In the estimates of the slabs made with CRFA, the EHE 08 [2] and CEB-FIB MC [4] standards were used and the results were also conservative and reduced the shear strength on average, 41% when comparing the experimental results to the EHE 08 standard [2] and 39% when compared to the results estimated by the MC [4]. In the slabs reinforced with CRFA, the differences between the estimates and the experimental results were even more conservative when analyzing the slabs with greater distances between the ribs (), l_0that is, with a larger cover area, especially L8, whose experimental result was 99% higher than that estimated by EHE 08 [2].

6 CONCLUSIONS

The results of this study lead to the conclusion that the slabs executed with conventional concrete followed the pattern of higher strength for the smallest distances between ribs (l_0), and the explanation is that for the higher spacing between ribs there were greater vertical displacements of the layers, twisting the ribs and shortening the shear failure. For the slabs reinforced with CRFA, it was observed that all of them presented a gain in shear strength, and this phenomenon occurred due to the reinforcement with CRFA increasing the stiffness of the layer and the contribution of the residual stress of CRFA in the fight against cracking, minimizing the effects of torsion on the ribs. The layers with CRFA contributed to the shear strength more effectively than the layers made of C30 class concrete. None of the slabs reached the conventional deformation limit of the normative

flexural rupture concrete of 3.5‰. On the upper surface of all slabs there was a cracking pattern at the layer-rib abutment, corroborating the normative prescriptions for verification of the flexural layer in ribbed slabs with excessive distance between the ribs. All the analyzed standards estimated shear strengths lower than the results found experimentally, underestimating these results by up to 60% by ACI 318 [1] and 50% by EHE 08 [2] for slabs without and with CFRA, respectively.

ACKNOWLEDGMENTS

The authors thank IPEAM for the financial support in all stages of the work.

REFERENCES

Alves, M. M. D. S. (2017). Potencial biotecnológico de bactérias e leveduras isoladas da casca do coco-verde (Cocos nucifera) em fermentação (Tese de Doutorado). Instituto de Química e Biotecnologia, Universidade Federal de Alagoas, Maceió.

Anagnostakis, S. L., & Hankin, L. (1975). Use of selective media to detect enzyme production by microorganisms in food products. Journal of Milk and Food Technology, 38(10), 570–572.

Barbosa, P. M. G., et al. (2020). Leveduras selvagens isoladas do caldo de cana com perfil para a produção de enzimas. Revista da Universidade Vale do Rio Verde, 17(2).

Bonfim, F. S. (2014). Diversidade de leveduras endofíticas em plantas medicinais (Dissertação de Mestrado). Universidade Federal de Pernambuco, Recife.

Borzani, W., et al. (2001). Biotecnologia industrial (v. 2). São Paulo: Edgard Blücher.

Buzzini, P., & Martini, A. (2002). Extracellular enzymatic activity profiles in yeast and yeast-like strains isolated from tropical environments. Journal of Applied Microbiology, 93(6), 1020–1025.

Cattelan, A. J. (1999). Métodos quantitativos para a determinação de características bioquímicas e fisiológicas associadas com bactérias promotoras de crescimento vegetal (36 p.). Londrina: Embrapa Soja.

Ceska, M. (1971). Enzyme catalysis of solidified media. European Journal of Biochemistry, 22(2), 186–192.

Chaplin, M. F., & Bucke, C. (1992). Enzyme technology. Cambridge: Cambridge University Press.

Cordeiro, C. A. M., Martins, M. L. L., & Luciano, A. B. (2002). Produção e propriedades da alfa-amilase do termofílico Bacillus sp. Revista Brasileira de Microbiologia, 33, 57–61.

Couto, F. M. M. (2008). Leveduras produtoras de β-glicosidase e pectinase (Dissertação de Mestrado). Universidade Federal de Pernambuco, Recife.

Farinas, C. S. (2011). A parede celular vegetal e as enzimas envolvidas na sua degradação (13 p.). São Carlos: Embrapa Instrumentação.

Gupta, R., et al. (2003). Microbial α-amylases: A biotechnological perspective. Process Biochemistry, 38(11), 1599–1616.

Hankin, L., & Anagnostakis, S. L. (1975). The use of solid media for detection of enzyme production by fungi. Mycologia, 67(3), 597–607.

Jay, J. M. (1992). Microbiologia moderna dos alimentos (3ª ed.). Zaragoza: Acribia.

Koelsch, G., et al. (2000). Enzymic characteristics of secreted aspartic proteases of Candida albicans. Biochimica et Biophysica Acta, 1480(1–2), 117–131.

Kumar, A., et al. (2023). Industrial applications of fungal lipases: A review. Frontiers in Microbiology, 14, 1142536. https://doi.org/10.3389/fmicb.2023.1142536

Kurtzman, C. P., & Fell, J. W. (Eds.). (1998). The yeasts: A taxonomic study (4ª ed., rev. and enl., v. 1). Amsterdam: Elsevier.

Lin, J. E., Chang, D. C. N., & Shen, G. J. (1991). Correlations among several screening methods used for identifying wood-decay fungi that can degrade toxic chemicals. Biotechnology Techniques, 5(5), 275–280.

Machado, M. A. A. (2015). Isolamento e seleção de leveduras para produção de enzimas de interesse industrial a partir de frutos do Cerrado (Dissertação de Mestrado em Biotecnologia). Universidade Católica Dom Bosco, Campo Grande.

Maijala, P., Fagerstedt, K. V., & Raudaskoski, M. (1991). Detection of extracellular cellulolytic and proteolytic activity in ectomycorrhizal fungi and Heterobasidion annosum. New Phytologist, 117(4), 643–648.

Melo, W. G. P., et al. (2019). Interações simbióticas entre microrganismos e insetos. RG News, 5(1), 48–56.

Moreira, F. M. S., & Siqueira, J. O. (2006). Microbiologia e bioquímica do solo (2ª ed., v. 1). Lavras: UFLA.

Motta, J. F. G., et al. (2023). Use of enzymes in the food industry: A review. Food Science and Technology, 43, e106222. https://doi.org/10.1590/fst.106222

Oliveira, A. N. D., et al. (2006). Enzimas hidrolíticas extracelulares de isolados de rizóbia nativos da Amazônia Central. Ciência e Tecnologia de Alimentos, 26(4), 853–860.

Peixoto, A. B. (2006). Estudo da produção de enzimas e gomas por leveduras selvagens coletadas em diversas regiões do Brasil (Dissertação de Mestrado). Universidade Estadual de Campinas, Campinas.

Raju, E. V. N., & Divakar, G. (2013). Screening and isolation of pectinase producing bacteria from various regions of Bangalore. International Journal of Pharmaceutical and Biomedical Research, 4(1), 151–154.

Ribeiro Júnior, J. C. (2015). Isolamento e identificação da microbiota esporulada e fúngica associada à deterioração do leite (Dissertação de Mestrado em Ciência Animal). Universidade Estadual de Londrina, Londrina.

Rodarte, M. P. (2005). Atividade proteolítica de bactérias, leveduras e fungos isolados dos frutos e grãos de café (Coffea arabica L.) (Dissertação de Mestrado). Universidade Federal de Lavras, Lavras.

Santos, T. T., et al. (2019). The digestive tract of Phylloicus (Trichoptera: Calamoceratidae) harbours different yeast taxa in Cerrado streams, Brazil. Symbiosis, 77(2), 147–160. https://doi.org/10.1007/s13199-018-0577-9

Silva, B. N., et al. (2023). Fungi from the body surface of Spodoptera frugiperda (Lepidoptera: Noctuidae) and bioassay of insecticidal activity. Observatorio de la Economía Latinoamericana, 21(9), 13647–13671. https://doi.org/10.55905/oelv21n9-170

Silva, E. M., et al. (2024). Investigation of the presence and enzymatic activity of fungi in stored corn (Zea mays L.) and soybean (Glycine max (L.) Merrill) grains. Caderno Pedagógico, 21(4), 1–21. https://doi.org/10.54033/cadpedv21n4-062

Sohail, M., et al. (2022). Cellulolytic and xylanolytic enzymes from yeasts: Properties and industrial applications. Molecules, 27(12), 3783. https://doi.org/10.3390/molecules27123783

Spencer, J. F., & Spencer, D. M. (1996). Maintenance and culture of yeasts. Methods in Molecular Biology, 53, 5–15.

Spier, M. R. (2005). Produção de enzimas amilolíticas fúngicas α-amilase e amiloglucosidase por fermentação (Dissertação de Mestrado). Universidade Federal do Paraná, Curitiba.

Stamford, T. L. M., Araújo, J. M., & Stamford, N. P. (1998). Atividade enzimática de microrganismos isolados do jacatupé (Pachyrhizus erosus L. Urban). Ciência e Tecnologia de Alimentos, 18(4).

Strauss, M. L. A., et al. (2001). Screening for the production of extracellular hydrolytic enzymes by non-Saccharomyces wine yeasts. Journal of Applied Microbiology, 91(1), 182–190.

Sukmawati, D., et al. (2023). The potential of cellulolytic yeast Pichia manshurica UNJCC Y-123, Saccharomyces cerevisiae UNJCC Y-84, and Saccharomyces cerevisiae UNJCC Y-83 to produce cellulase enzyme. Trends in Sciences, 20(10), 1–15. https://doi.org/10.48048/tis.2023.6950

Tavafi, H., et al. (2017). Screening of alginate lyase-producing bacteria and optimization of medium composition for extracellular production. Iranian Biomedical Journal, 21(1), 48–56.

Teixeira, M. F. N. P., Souza, C. R., & Morais, P. B. (2022). Diversity and enzymatic capabilities of fungi associated with the digestive tract of larval stages of a shredder insect in Cerrado and Amazon Forest, Brazil. Brazilian Journal of Biology, 82, e260039.

Wanderley, K. J., et al. (2004). Caracterização bioquímica da α-amilase da levedura Cryptococcus flavus. FEMS Microbiology Letters, 231(2), 165–169.

Zaky, A. S., et al. (2014). Marine yeast isolation and industrial application. FEMS Yeast Research, 14(6), 813–825. https://doi.org/10.1111/1567-1364.12158

APPENDIX

Figure 1

Forces acting on an inclined crack

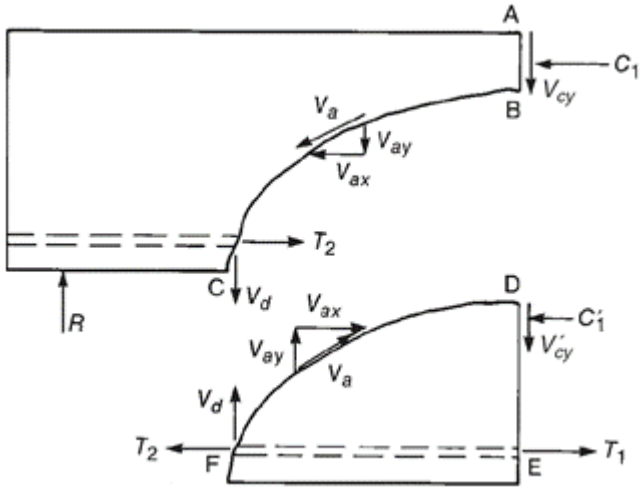

Source: MACGREGOR, 1997.

Figure 2

Effort transfer mechanism

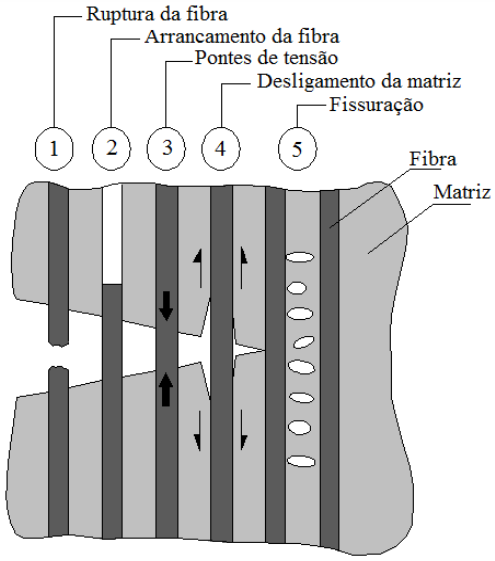

Source: adapted from GARCEZ, 2005.

Figure 3

Flexion model of the CEB-FIP Model Code (2010)

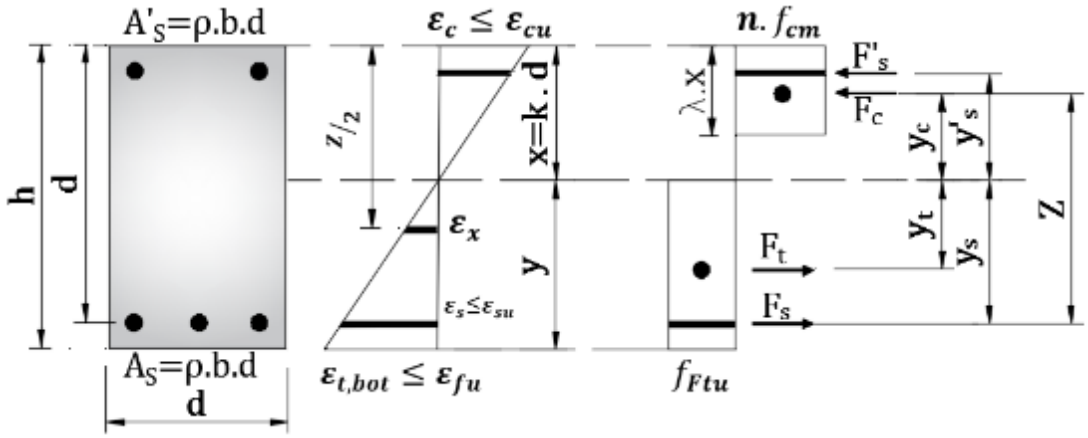

Source: CEB-FIP Model Code (2010).

Figure 4

Reinforcement of the slabs

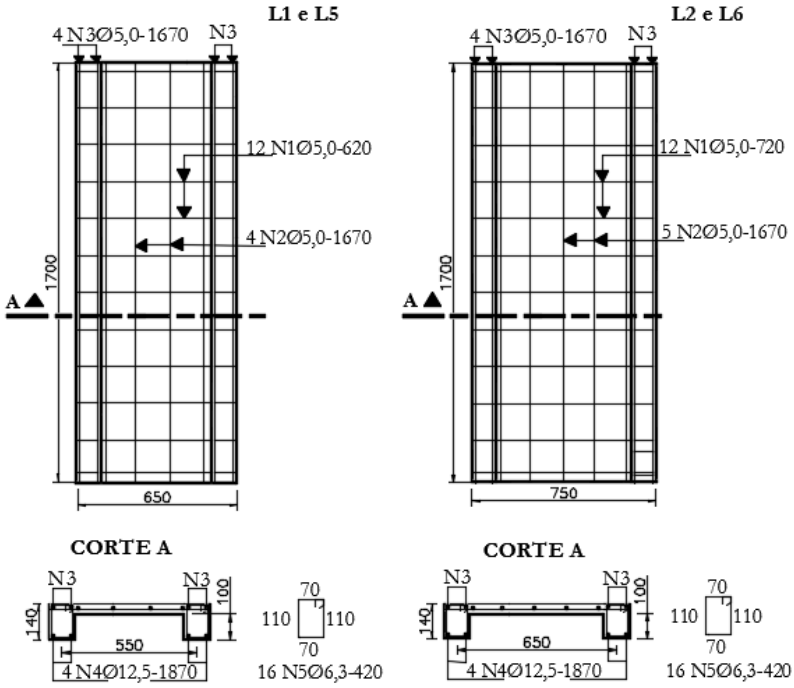

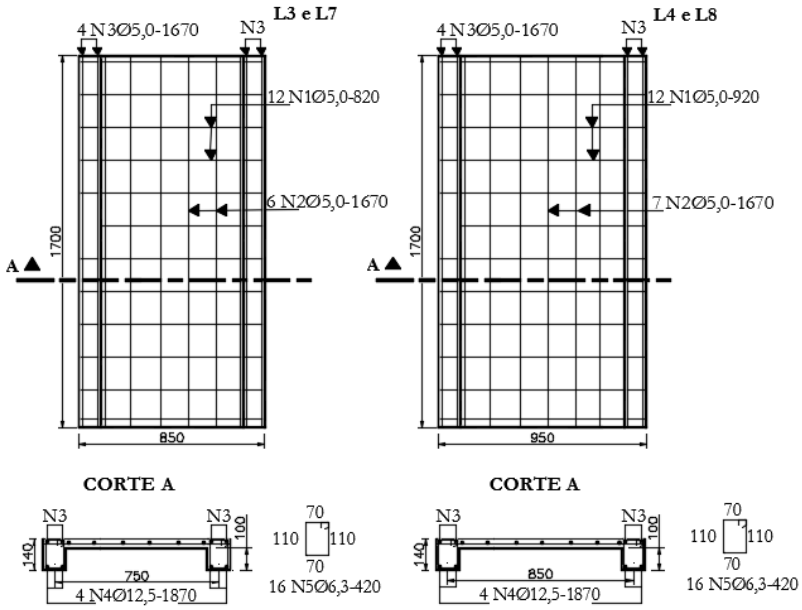

Source: The authors.

Figure 5

Rib reinforcements

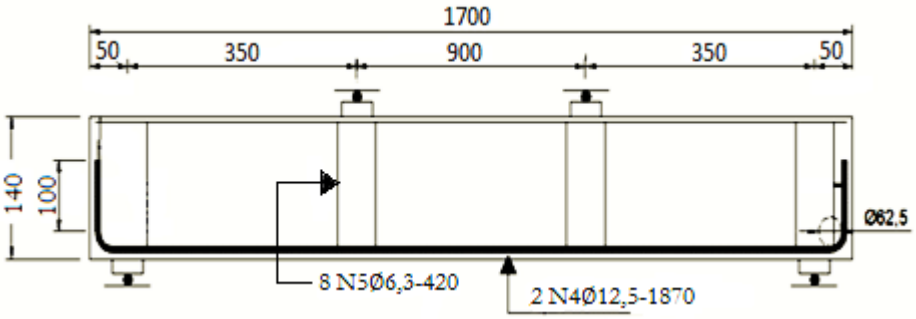

Source: The authors.

Figure 6

Crimped fiber used in CRFA

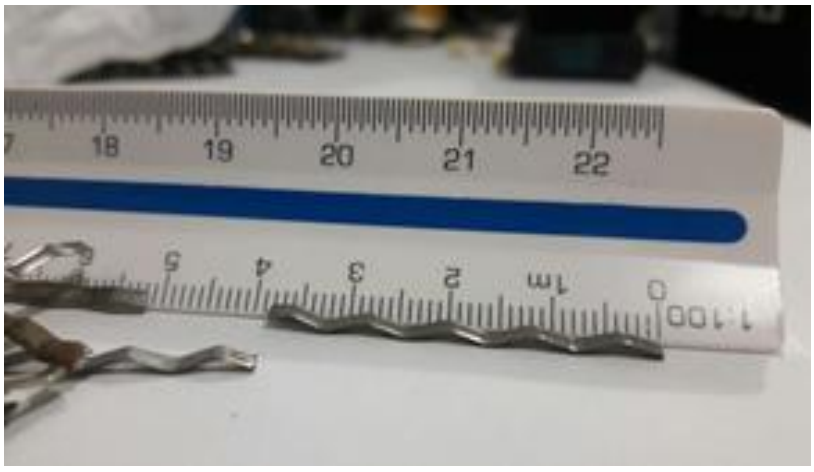

Source: The authors.

Figure 7

a) Arrangement for concreting b) Execution of the reinforcement, c) Regularization of the surface, d) Regularized surface

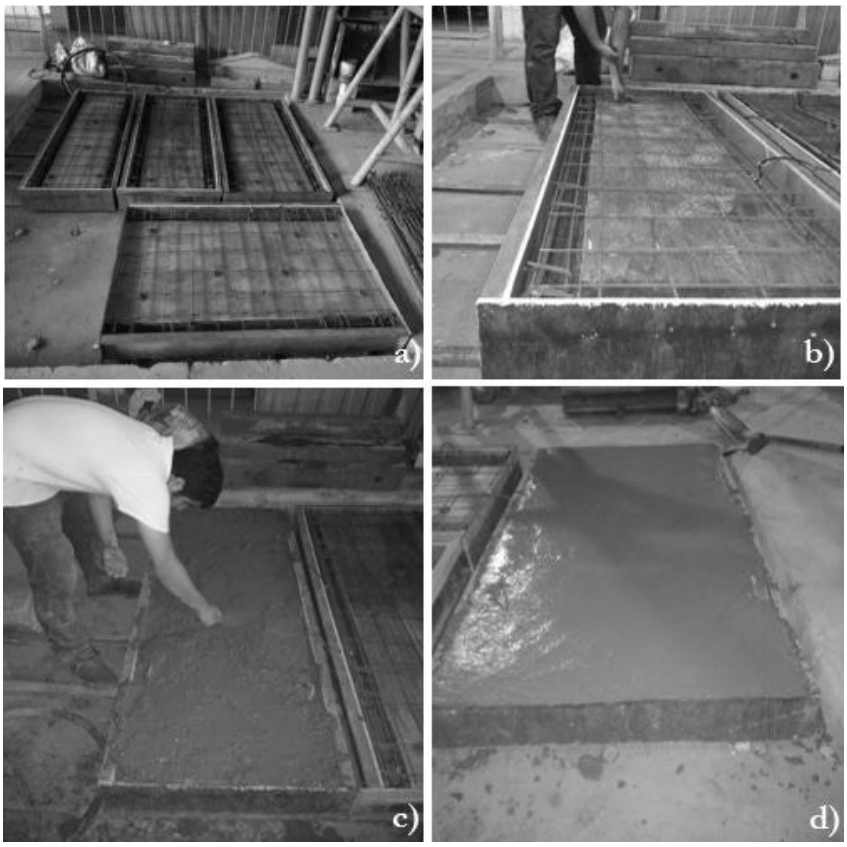

Source: The authors.

Figure 8

Position of the indicator clocks (D1 to D3) and extensometers on the covers (E1) and reinforcement of the ribs (E2) of the slabs

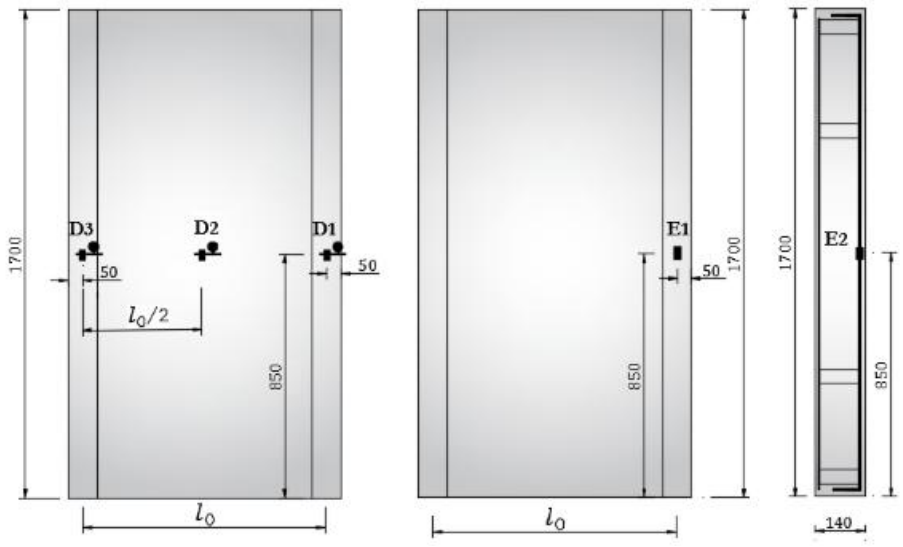

Source: The authors.

Figure 9

Details of the test system

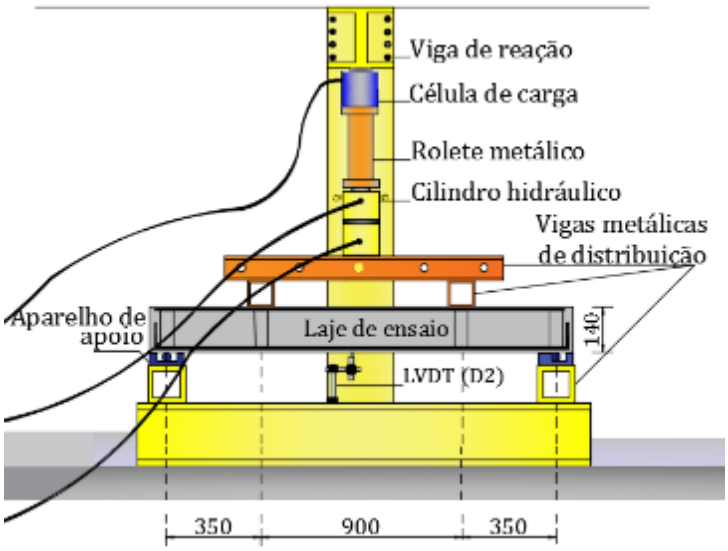

Source: The authors.

Figure 10

Maximum vertical displacements of the slabs

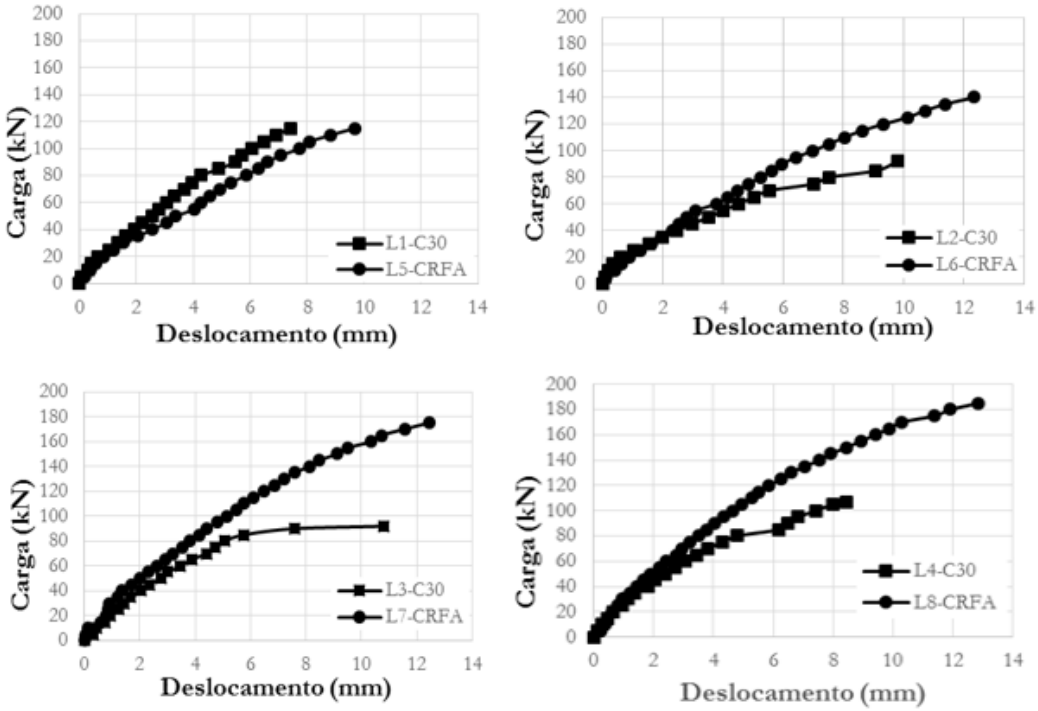

Source: Elaboration by the author (2020).

Figure 11

Deformations in the bending reinforcements of the ribs

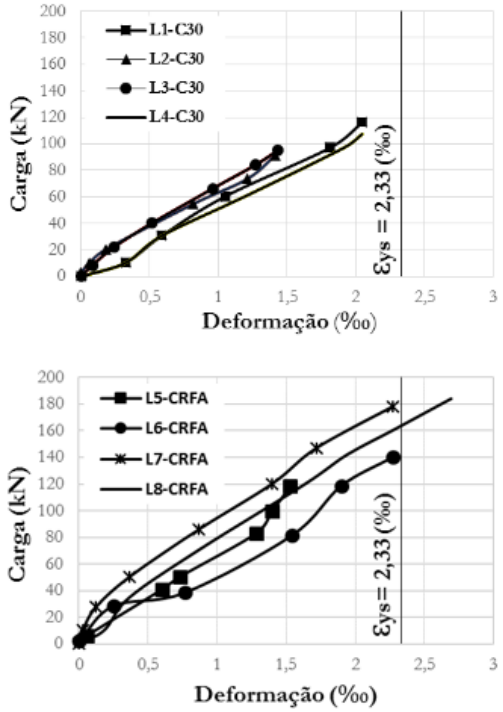

Source: Elaboration by the author (2020).

Figure 12

Appearance of the ribbed slabs after the tests

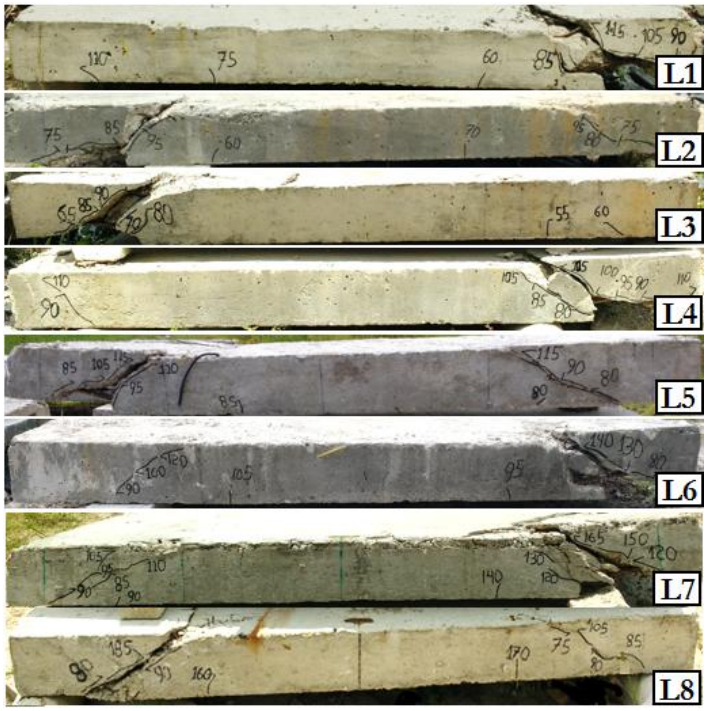

Source: The authors.

Figure 13

Breaking loads

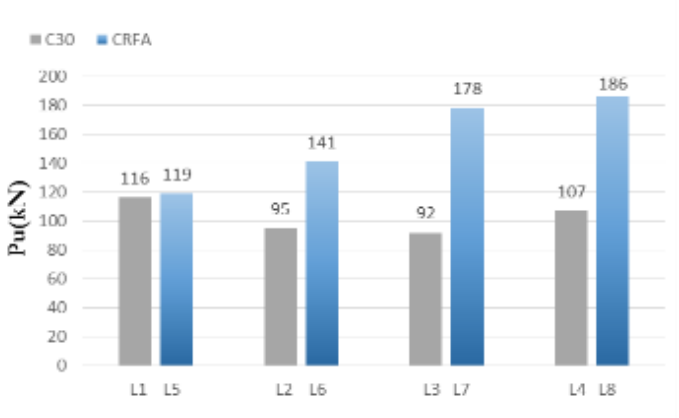

Source: Elaboration by the author (2020).

Table 1

Characteristics of the slabs

Slab	l_0(mm)	Group	f_c(MPa)
L1	550	C30	30
L2	650		28
L3	750		27
L4	850		31
L5	550	CRFA 1%	33
L6	650		33
L7	750		33
L8	850		32

Source: Elaboration by the author (2020).

Table 2

Mechanical properties of concrete.

Slab	Age	f_c	f_t	E_c
	(Days)	(MPa)	(MPa)	(GPa)
L1	54	30,0	2,9	19,1
L2	49	28,0	2,8	18,4
L3	64	27,0	2,8	19,4
L4	60	31,0	3,0	19,4
L5	56	31,0	3,1	20,3
L6	70	32,0	3,2	21,8
L7	68	33,0	3,4	23,2
L8	74	33,0	3,7	24,9

Source: Elaboration by the author (2020).

Table 3

Loads and failure modes of the slabs

Slab	l_0 (mm)	Group	$\varepsilon_{s,max}$ (‰)	$\varepsilon_{c,max}$ (‰)	P_u (kN)	P_{FLEX}/P_u	Burst mode
L1	550	C30	2,02	1,10	116,1	1,52	Ribbed shear.
L2	650		1,41	0,33	95,0	1,85	
L3	750		1,43	0,26	91,8	1,92	
L4	850		2,04	0,55	107,5	1,64	
L5	550	CRFA 1%	1,84	0,32	118,8	1,48	
L6	650		2,27	1,10	140,4	1,25	
L7	750		2,28	0,48	178,7	0,98	
L8	850		2,69	0,59	186,3	0,94	

Source: Elaboration by the author (2020).

Table 4

Estimated and experimental last loads

Slab	l_0 (mm)	Group	P_u (kN)	P_{NBR} (kN)	P_{ACI} (kN)	P_{EHE} (kN)	P_{CEB} (kN)	$\frac{P_U}{P_{NBR}}$ (kN)	$\frac{P_U}{P_{ACI}}$ (kN)	$\frac{P_U}{P_{EHE}}$ (kN)	$\frac{P_U}{P_{CEB}}$ (kN)
L1	550	C30	116,1	70,8	46,2	64,1	69,5	1,64	2,51	1,81	1,67
L2	650		95	66,0	44,7	62.7	67,2	1,44	2,12	1,51	1,41
L3	750		91,8	53,5	44,1	61,9	66,0	1,71	2,08	1,48	1,39
L4	850		107,5	57,3	47,1	64,8	66,7	1,87	2,28	1,65	1,61
L5	550	CRFA 1%	118,8			92,2	96,0			1,28	1,23
L6	650		140,4			92,9	96,0			1,51	1,46
L7	750		178,7			92,9	96,0			1,92	1,86
L8	850		186,3			93,6	96,0			1,99	1,94

Source: Elaboration by the author (2020).

Table 5

Flexural strength

$x\ (mm)$	27,40
z	102,79
ε_c (‰)	3,50
ε_{fu} (‰)	43,96
ε_s (‰)	11,03
ε'_s (‰)	1,18
$f_{ftu}\ (MPa)$	0,71
$f_s\ (MPa)$	570,00

$f'_s\ (MPa)$	248,13
$y_c\ (mm)$	16,44
$y_t\ (mm)$	56,30
$y_s\ (mm)$	86,35
$y'_s\ (mm)$	9,25
$F_c\ (kN)$	328,80
$F_t\ (kN)$	16,08
$F_s\ (kN)$	280,4
$F'_s\ (kN)$	31,0
$\sum F$	0,00
$m_R\ (kN.mm)$	30,8
$P_{FLEX}\ (kN)$	175,8

Source: Elaboration by the author (2020).